the surface is stretched by two identical and opposite forces with the velocity $U_w = -ax/(ct-1)$. The flow field is subjected by the external uniform magnetic field of strength B_0 in the direction of y-axis which generates magnetic field in the direction of x-axis. The recreation is performed by combination of graphene+water into dusty nanofluid. We considered spherical shape nano and dust particles. The number density of the dust particles is supposed to be stable and the volume fraction of dust particles is ignored in the entire flow problem. The drag force is considered into account for the particles and fluid interaction. Stokes linear drag theory is taken into account to model the drag force. The wall and the ambient temperatures are T_w and T_∞, respectively.

The constitutive equation for a Carreau fluid is given by (Raju et al. [20], Malik et al. [32]);

$$\tau = \eta_\infty + (\eta_0 - \eta_\infty)\left[1 + \left(\Gamma\dot{\gamma}\right)^2\right]^{0.5(n-1)}$$

$$\dot{\gamma} = \sqrt{\frac{1}{2}\sum\sum \dot{\gamma}_{ij}\dot{\gamma}_{ji}} = \sqrt{\frac{1}{2}\Pi}$$

Here, Π is the second invariant strain tensor.

According to the above assumptions, the physical governing system can be expressed as (Krishnamurthy et al. [22] , Sibanda and Makinde [33], Mebarek-Oudina [34] and Hayat et al. [35]):

$$\frac{\partial u}{\partial x} = -\frac{\partial v}{\partial y} \tag{1}$$

$$\frac{\partial u_p}{\partial x} = -\frac{\partial v_p}{\partial y} \tag{2}$$

$$(1-\phi_d)\rho_{nf}\left(\frac{\partial u}{\partial t} + u\frac{\partial u}{\partial x} + v\frac{\partial u}{\partial y}\right) = \mu_{nf}(1-\phi_d)\frac{\partial^2 u}{\partial y^2} + \left(\mu_f\frac{3(n-1)}{2}\Gamma^2\left(\frac{\partial u}{\partial y}\right)^2\left(\frac{\partial^2 u}{\partial y^2}\right) + KN(u_p-u) - \sigma B_0^2 u - \frac{\vartheta}{k_0}u\right) \tag{3}$$

$$\frac{\partial u_p}{\partial t} + u_p\frac{\partial u_p}{\partial x} + v_p\frac{\partial u_p}{\partial y} = \frac{K}{m}(u-u_p) \tag{4}$$

$$(\rho c_p)_{nf}\left(\frac{\partial T}{\partial t} + u\frac{\partial T}{\partial x} + v\frac{\partial T}{\partial y}\right) + \left(\lambda\left(u^2\frac{\partial^2 T}{\partial x^2} + v^2\frac{\partial^2 T}{\partial y^2} + \left(u\frac{\partial u}{\partial x} + v\frac{\partial u}{\partial y}\right)\frac{\partial T}{\partial x} + \left(2uv\frac{\partial^2 T}{\partial x\partial y} + \left(u\frac{\partial v}{\partial x} + v\frac{\partial v}{\partial y}\right)\frac{\partial T}{\partial y}\right)\right)\right) = \left(k_{nf}\frac{\partial^2 T}{\partial y^2}\right) - \frac{\partial q_r}{\partial y} + \frac{k_f U_w(x)}{xv_f}\left(A^*f'(T_w - T_\infty) + B^*(T-T_\infty)\right) + \left(\frac{Nc_{pf}}{\tau_T}(T_p - T) + \frac{N}{\tau_v}(u_p - u)^2\right) \tag{5}$$

$$\frac{\partial T_p}{\partial t} + u_p\frac{\partial T_p}{\partial x} + v_p\frac{\partial T_p}{\partial y} = -\frac{c_{pf}}{c_{mf}\tau_T}(T_p - T). \tag{6}$$

Based on the physical problem the boundary restrictions are [36]

$$\begin{aligned} &at\ y = 0,\ \ u = U_w, v = 0, h_f\frac{\partial T}{\partial y} = -k_f(T_w - T)\\ &as\ y\to\infty,\ \ u\to 0, u_p\to 0, v_p\to v, T\to T_\infty. \end{aligned} \tag{7}$$

The radiative heat flux is given by

$$q_r = -\frac{16\sigma^* T_\infty^3}{3K^*}\frac{\partial T}{\partial y}. \tag{8}$$

The thermophysical properties of nanofluids are given by

$$\left.\begin{aligned} &\rho_{nf} = (1-\phi)\rho_f + \phi\rho_s,\ (\rho c_p)_{nf} = (1-\phi)(\rho c_p)_f\\ &+\phi(\rho c_p)_s,\ \mu_{nf}\frac{\mu_f}{(1-\phi)^{2.5}},\ \frac{k_{nf}}{k_f} = \frac{(k_s + 2k_f) - 2\phi(k_f - k_s)}{(k_s + 2k_f) + \phi(k_f - k_s)},\\ &(\rho\beta)_{nf} = (1-\phi)(\rho\beta)_f + \phi(\rho\beta)_s. \end{aligned}\right\} \tag{9}$$

To transfer the governing equations into a set of ordinary differential equations, we introduce the following transformation as,

$$\begin{aligned} &u = \frac{ax}{1-ct}f'(\zeta), v = -\left(\frac{av_f}{1-ct}\right)^{(0.5)}f(\zeta), u_p = \frac{ax}{1-ct}F'(\zeta),\\ &v_p = -\left(\frac{av_f}{1-ct}\right)^{(0.5)}F(\zeta), \zeta = \left(\frac{a}{v_f(1-ct)}\right)^{(0.5)}y,\\ &T = (T_w - T_\infty)\theta(\zeta) + T_\infty, T_p = (T_w - T_\infty)\theta_p(\zeta) + T_\infty. \end{aligned} \tag{10}$$

3 Method of Solution

By substituting equations in (10) into Eqs. (1)–(6) along with boundary conditions (7), Eqs. (1) and (2) are automatically satisfied, Eqs. (3)–(7) are transformed as follows:

$$\frac{(1-\phi_d)}{(1-\phi)^{2.5}}\frac{d^3 f}{d\zeta^3} - \left(1-\phi+\phi\left(\frac{\rho_s}{\rho_f}\right)\right)(1-\phi_d)\left[A\frac{df}{d\zeta} + \frac{A\zeta}{2}\frac{d^2 f}{d\zeta^2} + \left(\frac{df}{d\zeta}\right)^2 - f\frac{d^2 f}{d\zeta^2}\right] + \left(\frac{3(n-1)}{2}We\left(\frac{d^2 f}{d\zeta^2}\right)^2\frac{d^3 f}{d\zeta^3} - (M+K)\frac{df}{d\zeta}\right) + \alpha\beta_v\left[\frac{dF}{d\zeta} - \frac{df}{d\zeta}\right] = 0 \tag{11}$$

Author's personal copy

$$F\frac{d^2 F}{d\zeta^2} - \frac{\Lambda}{2}\left[2\frac{dF}{d\zeta} + \zeta\frac{d^2 F}{d\zeta^2}\right] - \left[\frac{dF}{d\zeta}\right] + \beta_v\left[\frac{df}{d\zeta} - \frac{dF}{d\zeta}\right] = 0 \tag{12}$$

$$\left(1-\phi+\phi\left(\frac{(\rho c_p)_s}{(\rho c_p)_f}\right)\right)\left[\frac{\Lambda}{2}\zeta\frac{d\theta}{d\zeta} - f\frac{d\theta}{d\zeta}\right] + \Lambda\left[f^2\frac{d^2\theta}{d\zeta^2} + \frac{d\theta}{d\zeta}f'\frac{df}{d\zeta}\right] = \left[\frac{k_{nf}}{k_f} + {}^4/_3R\right]\left(\frac{1}{\Pr}\frac{d^2\theta}{d\zeta^2}\right) + A^*f' + B^*\theta + \frac{I\beta_T}{m}(\theta_p - \theta) + \frac{IEc\beta_v}{m}\left[\frac{dF}{d\zeta} - \frac{df}{d\zeta}\right]^2 \tag{13}$$

$$\frac{d\theta_p}{d\zeta}F(\zeta) - \gamma\beta_T(\theta_p(\zeta) - \theta(\zeta)) + \left[\frac{A}{2}\zeta\frac{d\theta}{d\zeta} - f\frac{d\theta}{d\zeta}\right] = 0. \tag{14}$$

The transformed boundary conditions are

$$\begin{aligned} &f'(0) = 1,\ \ f(0) = 0, \theta'(0) = -Bi(1-\theta(0))\\ &f'(\infty) = 0, F'(\infty) = 0, F(\infty)\to -f(\infty), \theta(\infty) = 0, \theta_p(\infty) = 0 \end{aligned} \tag{15}$$

where A, We, M, K, α, β_v, $\Pr$, Q_H, l, β_T, Ec, R, γ, τ_v are specified as

$$\begin{aligned} &A = \frac{c}{a}, We = \frac{\Gamma^2 a^3 x^2}{v_f(1-ct)^3}, K = \frac{v(1-ct)}{k_0\rho_f a}, M = \frac{\sigma B_0^2(1-ct)}{a\rho_f},\\ &Bi = \frac{k_f}{ah_f(1-ct)}, \alpha = \frac{Nm}{\rho_f}, \beta_v = \frac{1-ct}{a\tau_v}, \Pr = \frac{(\mu c_p)_f}{k_f},\\ &l = \frac{mN}{\rho_f}, \beta_T = \frac{1-ct}{a\tau_T}, Ec = \frac{u_w^2}{(T_w - T_\infty)(c_p)_f}, \Lambda = \frac{\lambda a}{1-ct},\\ &R = \frac{4\sigma^* T_\infty^3}{k^* k_f}, \gamma = \frac{(c_p)_f}{c_{mf}}, \tau_v = \frac{m}{k}. \end{aligned} \tag{16}$$

4 Numerical Solutions

The non-linear differential Eqs. (11)–(14) with the boundary limitations (15) are numerically solved using Runge-Kutta with shooting method. Initially, the set of non-linear differential equations are transformed into first-order differential equations by using the following process:

$$\begin{aligned} &f = y_1, \frac{df}{d\zeta} = y_2, \frac{d^2 f}{d\zeta^2} = y_3, F = y_4, \frac{dF}{d\zeta} = y_5, \theta = y_6, \theta'\\ &= y_7, \theta_p = y_8, \end{aligned} \tag{17}$$

$$y_3' = \left(\frac{1}{\left(\frac{1}{(1-\phi_d)/(1-\phi)^{2.5}} + \frac{3(n-1)}{2}We y_3^2\right)}\right)\left(\begin{aligned} &(1-\phi_d)\left(1-\phi+\phi\left(\frac{\rho_s}{\rho_f}\right)\right)\\ &\left(Ay_2 + A\frac{\zeta}{2}y_3 + y_2^2 - y_1y_3\right)\\ &+(M+K)y_2 - \alpha\beta_v(y_5 - y_2) \end{aligned}\right), \tag{18}$$

$$y_5' = ((A+1)y_2 - \beta_v(y_2 - y_5))\left(\frac{1}{y_4 - \zeta A/2}\right), \tag{19}$$

$$y_7' = \left(\frac{k_{nf}}{k_f}\frac{1}{\Pr} + \frac{4}{3}\frac{R}{\Pr} - \Lambda y_1^2\right)\left(\begin{aligned} &\left(\zeta\frac{A}{2}y_7 - \gamma_1 y_7\right)\left(1-\phi+\phi\frac{(\rho c_p)_s}{(\rho c_p)_f}\right) + \Lambda y_2 y_1 y_2\\ &-\frac{I\beta_T}{m}(y_8 - y_6) - A^* y_2 - B^* y_6 + \frac{IEc\beta_v}{m}(y_5 - y_2)^2 \end{aligned}\right), \tag{20}$$

$$y_8' = (\gamma\beta_T(y_8 - y_6))(1/y_4). \tag{21}$$

With boundary conditions as

$$\begin{aligned} &y_2 = 0, y_1 = 0, y_7 = Bi(1-y_6),\ \text{at}\ \zeta\to 0\\ &y_2 = 0, y_5 = 0, y_4 = -y_1, y_6 = 0, y_8 = 0\ \text{at}\ \zeta\to\infty. \end{aligned} \tag{22}$$

We guess the values of $y_3(0)$, $y_4(0)$, $y_5(0)$, $y_7(0)$ which are not specified at the initial conditions. Equations (18)–(21) are integrated Runge-Kutta method with the step length is 0.01. The accuracy of the considered values is checked by equating the calculated values of $y_2, y_4 y_5, y_6, y_8$ at $\zeta = \zeta_{\max}$ with their given values at $\zeta = \zeta_{\max}$. If there exists any difference, the procedure is continued up to the required good values. Alternatively, we are using the Runge-Kutta Feldberg method to get the accurately obtained initial values of y_2, y_4, y_5, y_6, y_8 and then integrate Eqs. (18)–(21) by using the Runge-Kutta method. This procedure is continued until the settlement between the designed value and the limitation given at is within the specified degree of accuracy 10^{-5}.

For the purpose of engineering interest, skin friction coefficient (C_f) and local Nusselt number (Nu_x) are defined as:

$$C_f\sqrt{\mathrm{Re}_x} = \left(\frac{3(n-1)}{2}We\left(\frac{d^2 f(0)}{d\zeta^2}\right)^2 + \frac{1}{(1-\phi)^{2.5}}\left(1 + \frac{1}{\beta}\right)\frac{d^2 f(0)}{d\zeta^2}\right) \tag{23}$$

$$\frac{Nu_x}{\sqrt{\mathrm{Re}_x}} = -\left(\frac{k_{nf}}{k_f}\right)\left(1 + \frac{4}{3}R\right)\theta'(0) \tag{24}$$

where $\mathrm{Re}_x = \left(\frac{U_w x}{v_f}\right)$ is local Reynolds number.

Author's personal copy

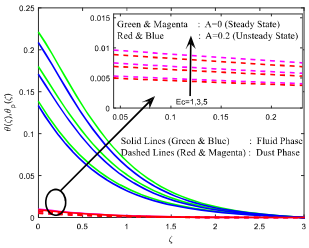

Fig. 2 Impact of Econ temperature in stretching case

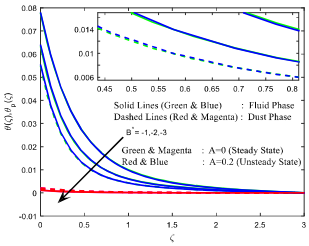

Fig. 4 Impact of B^* on temperature in stretching case

5 Result and Discussion

The non-dimensional governing Eqs. (11)–(14) subjected to boundary limitations (15) have been solved numerically using Runge-Kutta method with shooting technique. In order to obtain the results, numerical computations are carried out by considering different values of non-dimensional governing parameters as: $l = 2$, $m = 0.3$, $K = 0.5$, $\zeta = 1$, $\lambda = 0.3$, $R = 0.5$, $We = 0.2$, $n = 3$, $\phi_d = 0.01$, $\alpha = 0.2$, $\beta_v = 0.2$, $\beta_t = 0.2$, $Ec = 0.1$, these values remain unaltered throughout this analysis excluding some variations in respective figures and tables. In figures, solid line denotes the fluid phase profiles and dashed lines denote the dust phase profiles of the flow.

In Figs. 2, 3, 4, 5, 6, 7, 8, 9, 10, 11 and 12, we displayed the impact of the abovementioned non-dimensional parameter on temperature and velocity profiles over steady and unsteady stretching sheet. Figure 2 refers the impact of Ec on temperature profiles. Figure 13 displays the impact of R on temperature profiles. From this graph, we analyzed that the thermal radiation increases the temperature profiles. Figure 14 shows that the impact of magnetic parameter on velocity profiles. It is clear from this graph that the magnetic parameter reduces velocity profile. As increasing value of Eckert number amplifies the heat transfer dissipation, hence, we saw increment in temperature profile. It is noticed that the heat transfer on unsteady stretching sheet gains higher temperature profiles than steady stretching sheet. Figures 3 and 4 analyze the effect of A^* & B^* on temperature profiles, by these graphs we conclude that these two parameters strengthen temperature profiles, as these two parameters act like heat source/sink which generates thermal energy in the direction of flow. Comparing to heat transfer in unsteady stretching sheet, steady stretching sheet gains higher values as particles lose the thermal energy in unsteady stretching sheet than in steady stretching sheet. Figure 5 indicates the impact of Bi on temperature profiles, by this graph we conclude that Biot number amplifies the temperature profiles, in this case heat transfer on unsteady stretching sheet is lower than heat transfer of steady stretching

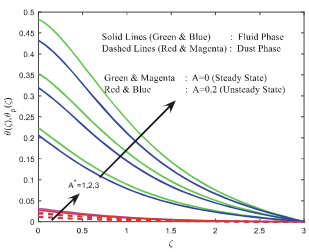

Fig. 3 Impact of A^* on temperature in stretching case

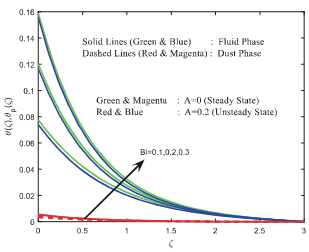

Fig. 5 Impact of Bi on temperature in stretching case

Author's personal copy

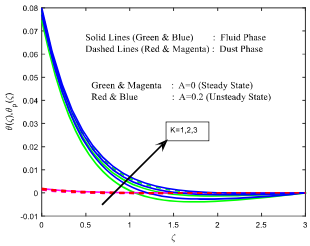

Fig. 16 Impact of K on temperature shrinking case

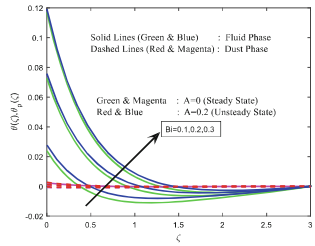

Fig. 19 Impact of Bi on temperature in shrinking case

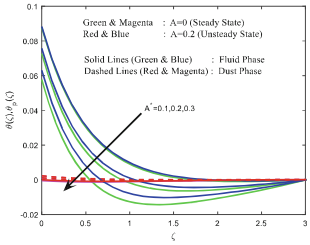

Fig. 17 Impact of A^* on temperature in shrinking case

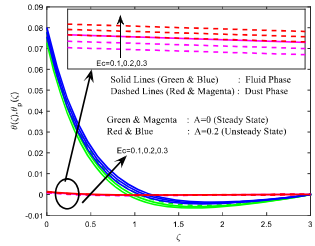

Fig. 20 Impact of Ec on temperature in shrinking case

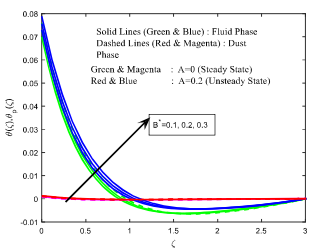

Fig. 18 Impact of B^* on temperature in shrinking case

Table 1 Justification of the local Nusselt number $-\theta'(0)$ for the case of$t = 1$, $A = A^* = 0 B^* = We = 0, l = M = K = \delta = A = \phi = \phi_d = \gamma = 0$

Pr	Present studies	Krishnamurthy [22]	Santhosh et al. [25]
0.72	1.088567	1.0885	1.08762
1.0	1.33333	1.3333	1.33334
10.0	4.7969	4.7968	4.77582

Table 2 Thermophysical properties of water and graphene are given by

Thermophysical properties	Water	Graphene
ρ (kg/m^3)	997	2250
C_p (J/kg K)	4179	2100
k (W/m K)	0.613	2500
Prandtl number	7.10	

velocity and temperature profiles over steady shrinking sheet gain lower values than velocity and temperature profiles over unsteady shrinking sheet. Figures 17 and 18 analyze the impact of A^* & B^* on temperature profiles, by these graphs, we reported that A^* reduces temperature profiles, and B^* amplifies the temperature profiles. The velocity and temperature profiles over unsteady shrinking sheet gains higher values compared to the steady shrinking sheet. The influence of Bi on temperature profiles has been shown in Fig. 19, by this graph, we analyzed that the effect of Biot number increases the temperature profiles. Compared to velocity and temperature profiles over steady shrinking sheet, the unsteady shrinking sheet takes higher values. Figure 20 pictures the impact of Ec on temperature profiles; by these graphs, we conclude that the Eckert number enriches temperature profiles.

Table 1 displays the justification of the present study with the already existing study under limited case. Table 2 shows the thermophysical properties of base fluid and graphene nanoparticles. Table 3 certifies the effect of various non-dimensional parameters on skin friction and local Nusselt number in case of steady and unsteady stretching sheet. This table summarizes as follows. The improved values of Ec do not show any variation in skin friction for both steady and unsteady stretching sheets, as we expected, these values decrement in the heat transfer rate due to domination of graphene particles in the flow. The improved values of A^*stabilize the skin friction of both the steady and unsteady stretching sheets and reduce the heat transfer rate. Similarly, the decreased values of B^* do not show any effect in skin friction of both steady and unsteady stretching sheets, but these improved values decrement the heat transfer rate, as A^* & B^* are obtained from non-uniform heat source/sink which acts as heat generator/absorber. The improved values of Bi stabilize the values of skin friction but these values decrement the heat transfer rate of both the steady and unsteady stretching sheets. The heat transfer rate is enriched by increasing the values of M but these values decrease the skin friction. The improved values of porosity decrement the skin friction and decrement heat transfer rate for both the steady and unsteady stretching sheets. The improved values of R stabilize the values of skin friction rate and reduce heat transfer rate in both the cases. As we expected, the improved values of We decrease skin friction and heat transfer rate.

Table 4 certifies the effect of various non-dimensional parameters on the skin friction and local Nusselt number in case of steady and unsteady shrinking sheets. This table summarizes as follows. The improved values of We enrich the skin friction and the heat transfer rate of both steady and unsteady shrinking sheets. The improved values of R do not show any effect on skin friction but these values decrement the heat transfer rate. The skin friction rate and heat transfer rate are enriched by the increased values of M. The decreased values of K increase the skin friction in both the steady and unsteady shrinking sheets, but these decreased values enrich the heat transfer rate in steady shrinking sheet and decrease the heat transfer rate in unsteady shrinking sheet. The improved values of A^* & B^* do not show any effect in the skin friction, but these values enrich heat transfer rate in both steady and unsteady cases. The improved values of Bi stabilize values of the skin friction but these values increment the heat transfer rate in both cases. The improved values Ec do not show any variation in the skin friction for both cases, but as we expected, these values decrement heat transfer rate due to domination graphene particles.

Table 3 The effect various non-dimensional parameters on skin friction (C_f) and local Nusselt number (Nu_s) in case of steady and unsteady stretching sheet

Ec	A^*	B^*	B_i	M	K	R	We	$-C_f$		Nu_s	
								Steady	Unsteady	Steady	Unsteady
1								0.251830	0.262523	0.193253	0.194442
3								0.251830	0.262523	0.183979	0.186011
5								0.251830	0.262523	0.174704	0.177581
	1							0.251829	0.262523	0.174141	0.178009
	2							0.251829	0.262523	0.145035	0.152725
	3							0.251830	0.262523	0.145035	0.127440
		−1						0.251829	0.262523	0.206962	0.206898
		−2						0.251829	0.262523	0.210176	0.210022
		−3						0.251829	0.262523	0.212120	0.211950
			0.1					0.251829	0.262523	0.103485	0.103909
			0.2					0.251829	0.262523	0.197427	0.198236
			0.3					0.251829	0.262523	0.283087	0.284250
				1				0.301482	0.309346	0.197785	0.198499
				2				0.388835	0.393033	0.198287	0.198880
				3				0.466885	0.468677	0.198631	0.199151
					1			0.301482	0.309346	0.197785	0.198499
					2			0.388835	0.393033	0.198287	0.198880
					3			0.466885	0.468677	0.198631	0.199151
						1		0.251829	0.262523	0.194634	0.195678
						2		0.251829	0.262523	0.190100	0.191509
						3		0.251829	0.262523	0.186445	0.188124
							1	0.290873	0.306091	0.197357	0.198176
							4	0.384578	0.409581	0.197173	0.198020
							7	0.445100	0.476020	0.197048	0.197916

Author's personal copy

Table 4 The effect various non-dimensional parameters on skin friction (C_f) and local Nusselt number (Nu_s) in case of steady and unsteady shrinking sheet

We	R	M	K	A^*	B^*	B_i	Ec	C_f		Nu_s	
								Steady	Unsteady	Steady	Unsteady
1								0.219718	0.239475	0.208126	0.207446
4								0.276539	0.307184	0.208245	0.207545
7								0.315980	0.353432	0.208331	0.207614
	1							0.198289	0.213354	0.204203	0.203976
	3							0.198289	0.213354	0.198122	0.198557
	5							0.198289	0.213354	0.193375	0.194284
		1						0.255080	0.265694	0.207652	0.207123
		2						0.349633	0.355335	0.207097	0.206731
		3						0.431367	0.434187	0.206736	0.206464
			−1					0.255080	0.265694	0.207652	0.207123
			−2					0.349633	0.355335	0.207097	0.206731
			−3					0.431367	0.434187	0.206736	0.206464
				0.1				0.198289	0.213354	0.204717	0.204588
				0.2				0.198289	0.213354	0.208083	0.207410
				0.3				0.198289	0.213354	0.211448	0.210231
					1			0.198289	0.213354	0.208695	0.208034
					2			0.198289	0.213354	0.208083	0.207410
					3			0.198289	0.213354	0.207374	0.206696
						1		0.198289	0.213354	0.109533	0.109090
						2		0.198289	0.213354	0.208083	0.207410
						3		0.198289	0.213354	0.297223	0.296479
							1	0.198289	0.213354	0.208083	0.207410
							2	0.198289	0.213354	0.207529	0.206925
							3	0.198289	0.213354	0.206976	0.206441

6 Conclusions

In most of the existing problems, the heat transfer characteristics of nanofluid or dusty fluids are revealed individually. For the first time, we proposed the combination of dusty and graphene over a stretching or shrinking surface with impact of magneto hydrodynamic unsteady Carreau fluid. The uniform and non-uniform heat generation or sink are also taken into account with porous layers. The simulation is performed by suspension of graphene nanoparticles into base water. The arising set of partial differential equations (PDEs) are transformed into set of ordinary differential equations (ODEs) using suitable similarity transformations, and then solved by the help of Runge-Kutta with shooting technique.

- The impact of Eckert number enriches the temperature profile for both steady and unsteady cases of stretching as well as shrinking sheet.
- The improved value of Weissenberg number enriches the skin friction and the heat transfer rate of both steady and unsteady cases of shrinking sheet. But reverse phenomena occurs in the case of stretching sheet.
- The Biot number increases the temperature profile for both steady and unsteady cases of stretching as well as shrinking sheet.
- The radiation amplifies the temperature profiles of both stretching and shrinking sheets; compared to shrinking sheet, stretching sheet gains higher values.